NASA/TM-20240013421

Influence of Actuator Movement Rate During Acquisition of Inlet Characterization Data

T. Shane Sowers
HX5, LLC, Brook Park, Ohio

Thomas J. Stueber
Glenn Research Center, Cleveland, Ohio

January 2025

NASA STI Program Report Series

Since its founding, NASA has been dedicated to the advancement of aeronautics and space science. The NASA scientific and technical information (STI) program plays a key part in helping NASA maintain this important role.

The NASA STI program operates under the auspices of the Agency Chief Information Officer. It collects, organizes, provides for archiving, and disseminates NASA's STI. The NASA STI program provides access to the NTRS Registered and its public interface, the NASA Technical Reports Server, thus providing one of the largest collections of aeronautical and space science STI in the world. Results are published in both non-NASA channels and by NASA in the NASA STI Report Series, which includes the following report types:

- TECHNICAL PUBLICATION.
  Reports of completed research or a major significant phase of research that present the results of NASA programs and include extensive data or theoretical analysis. Includes compilations of significant scientific and technical data and information deemed to be of continuing reference value. NASA counterpart of peer-reviewed formal professional papers but has less stringent limitations on manuscript length and extent of graphic presentations.

- TECHNICAL MEMORANDUM.
  Scientific and technical findings that are preliminary or of specialized interest, e.g., quick release reports, working papers, and bibliographies that contain minimal annotation. Does not contain extensive analysis.

- CONTRACTOR REPORT.
  Scientific and technical findings by NASA-sponsored contractors and grantees.

- CONFERENCE PUBLICATION.
  Collected papers from scientific and technical conferences, symposia, seminars, or other meetings sponsored or cosponsored by NASA.

- SPECIAL PUBLICATION.
  Scientific, technical, or historical information from NASA programs, projects, and missions, often concerned with subjects having substantial public interest.

- TECHNICAL TRANSLATION.
  English-language translations of foreign scientific and technical material pertinent to NASA's mission.

Specialized services also include organizing and publishing research results, distributing specialized research announcements and feeds, providing information desk and personal search support, and enabling data exchange services.

For more information about the NASA STI program, see the following:

- Access the NASA STI program home page at http://www.sti.nasa.gov

NASA/TM-20240013421

Influence of Actuator Movement Rate During Acquisition of Inlet Characterization Data

T. Shane Sowers
HX5, LLC, Brook Park, Ohio

Thomas J. Stueber
Glenn Research Center, Cleveland, Ohio

National Aeronautics and
Space Administration

Glenn Research Center
Cleveland, Ohio 44135

January 2025

Acknowledgments

The funding for this effort was supplied under the directed guidance of the NASA Hypersonic Technology Project by Project Manager Mary Jo Long-Davis of the NASA Glenn Research Center and Deputy Project Manager Andrea Storch of the NASA Langley Research Center.

This report contains preliminary findings, subject to revision as analysis proceeds.

This work was sponsored by the Advanced Air Vehicles Program at the NASA Glenn Research Center.

Level of Review: This material has been technically reviewed by technical management.

This report is available in electronic form at https://www.sti.nasa.gov/ and https://ntrs.nasa.gov/

NASA STI Program/Mail Stop 050
NASA Langley Research Center
Hampton, VA 23681-2199

Influence of Actuator Movement Rate During Acquisition of Inlet Characterization Data

T. Shane Sowers
HX5, LLC
Brook Park, Ohio 44142

Thomas J. Stueber
National Aeronautics and Space Administration
Glenn Research Center
Cleveland, Ohio 44135

Summary

This report considers using a process to acquire performance data for supersonic mixed-compression inlets that is faster and less costly than the previous process. In the previous process for acquiring data during wind tunnel experiments, actuators for backpressuring an inlet moved in discrete increments, paused for dynamics to dampen, measured data for 5 s, recorded the data, and then reduced the data to graphic plots of pressure recovery versus mass capture ratio. This discrete data acquisition procedure was methodical, reliable, and accurate. However, acquiring data to characterize the inlet consumed significant wind-on time. Wind tunnel operation was costly when considering maintenance, energy, and human resources (operators and research team); therefore, the price for each data point was high. This report presents a quicker method to obtain all measurements, one which can also be used in blowdown wind tunnels. This approach, identified as the dynamic inlet characteristic data acquisition procedure, uses in situ dynamic high-speed pressure sensors to measure pressure signals. The backpressuring actuator moves continuously, and measurements from high-speed pressure sensors are recorded as the actuator progresses to and past the incremental points. Despite its advantages, the approach raised the following questions: (1) Will the new process be as accurate as the previous process? and (2) Are there any hidden costs? These concerns are addressed in this report. This report reviews a study that was undertaken to compare wind tunnel experiment data taken using the previous discrete data acquisition procedure with data recorded using the dynamic inlet characterization data acquisition procedure. In this report, the wind tunnel experiment and the study objectives are described. The processes to reduce the data for analysis are explained, and a discussion of the results is given. Finally, conclusions from this study that may guide further work in this area are presented.

Nomenclature

AIP	aerodynamic interface plane
$C0_{Cold}$	cold calibration coefficient for bias
$C0_{Hot}$	hot calibration coefficient for bias
$C1_{Cold}$	cold calibration coefficient for slope
$C1_{Hot}$	hot calibration coefficient for slope
ESP	electronic scanned pressure
i	discrete working data point
j	sensor number
k	data point

m	number of data points in discrete working set
MFP	mass flow plug
P_{Cold}	measured pressure using cold calibration coefficients
P_{CP}	cold pipe static pressure
P_{Hot}	measured pressure using hot calibration coefficients
P_{Norm}	AIP total pressure normalizing value
P_{Recal}	recalibrated pressure measurement
$P_{T,AIP,j}$	AIP total pressure for sensor j
P_{T0}	freestream total pressure
P_{T2}	diffuser total pressure
re	total error
SDQ	sensor data qualification
SWT	supersonic wind tunnel
T_T	total temperature
$Volts$	volts measured from pressure sensor
W_2	cold pipe airflow rate
W_{Ref}	theoretical captured mass flow rate at inlet
X_{MFP}	mass flow plug position
$\Delta_{P,i}$	difference in pressure recovery for discrete working data point i
$\Delta_{W,i}$	difference in mass flow ratios for discrete working data point i

Introduction

This work considers a procedural change for improving data acquisition efficiencies while performing experiments in a wind tunnel to characterize the performance of a supersonic mixed-compression inlet system. This study focuses on the experimental process and data acquisition as well as reduction processes to populate plots of inlet pressure recovery versus mass capture ratio. These plots are called inlet characteristic curves and are also known as cane curves because the data plots resemble a canelike pattern. Each cane curve reveals inlet performance at a steady-state freestream condition and a specific inlet geometry. The proposed experimental methodology to replace the previous methodology suggests acquiring data without requiring the inlet to be in a near-steady-state condition.

This report is organized as follows. A brief overview of the inlet system and the wind tunnel that was used to acquire experimental data is presented. The cane curve plots produced by the experimental data are explained. The traditional method for populating cane curve plots is summarized, followed by a description of the proposed method associated with this work. The data reduction processes are specified, and results are presented and discussed. Potential future activities are suggested, followed by concluding remarks.

Inlet System

A supersonic mixed-compression inlet system was used to acquire experimental data. The system included a cold pipe and mass flow plug (MFP) at the aft end of the inlet, as illustrated in Figure 1. This type of inlet system compresses and decelerates freestream airflow for use by a turbine engine. As shown, airflow enters from the left into a convergent duct, passes through a throat area, and moves into a subsonic diffuser. Within the subsonic diffuser, a normal shock wave develops between incoming supersonic flow and downstream subsonic flow. Airflow from the subsonic diffuser is returned to freestream by way of venting through bypass doors or by passing through a cold pipe and then exiting through a choked MFP.

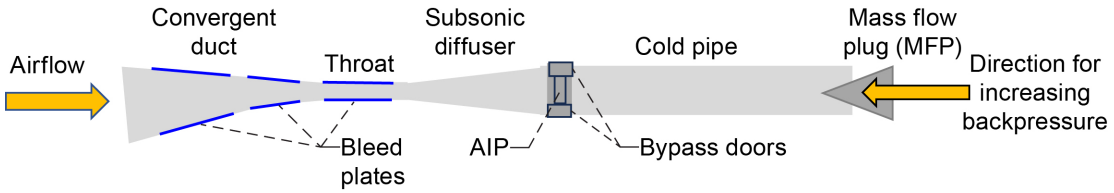

Figure 1.—Simplified diagram of supersonic mixed-compression inlet system.

In this study, the bypass doors and MFP were used to regulate conditions within the inlet system. The bypass doors would open as needed to vent airflow to the freestream and relieve subsonic diffuser backpressure. The junction where the cold pipe meets the subsonic diffuser was identified as the aerodynamic interface plane (AIP). In the started condition, the normal shock wave resided downstream from the throat and upstream from the AIP in the subsonic diffuser. Backpressure in the subsonic diffuser was increased by moving the MFP closer to the cold pipe exit to decrease the cold pipe exit area or by moving the bypass doors to more closed positions; either method resulted in the normal shock moving upstream. Likewise, backpressure was decreased by moving the MFP farther from the cold pipe to increase the cold pipe exit area or by moving the bypass doors to more open positions, resulting in the normal shock moving downstream.

The illustrated inlet system in Figure 1 is simplified and does not show variable geometry. Two examples of variable geometry would be (1) actuators to increase or decrease the freestream capture area and (2) actuators to increase or decrease the throat height. For inlet systems with variable geometry, performance characteristic curves are desired at all possible freestream operating conditions and inlet configurations.

The cold pipe and MFP were used to simulate the impact of a turbine engine on the backpressure buildup in the subsonic diffuser. An accelerating turbine engine was simulated by moving the MFP away from the aft end of the cold pipe. Likewise, a decelerating turbine engine was simulated by moving the MFP toward the aft end of the cold pipe.

The inlet system had multiple sets of bleed plates. The most upstream bleed plates were designed to reduce the boundary layer, thus allowing more airflow to the area where the turbine engine would be located. The throat bleed was employed as a passive stability control device. If the normal shock reached the throat bleed, the high-pressure air behind the normal shock would be vented to freestream through the throat bleed. The venting would relieve the backpressure, causing the normal shock to cease moving upstream and triggering an unstart. Actions to further increase the backpressure could move the normal shock upstream past the throat bleed plate.

For peak performance, the typical operating strategy for supersonic mixed-compression inlets has the normal shock located near the throat to reduce distortion at the face of the turbine engine. However, if the normal shock were located over the throat bleed, then high-pressure subsonic diffuser air would vent to freestream and would be accounted for as propulsion drag. Thus, the challenge is to keep the normal shock positioned as close as possible to, but not over, the throat bleed while maintaining constant mass flow to the MFP. This challenge was addressed by modulating bypass doors aft of the throat in order to vent high-pressure subsonic diffuser air to the freestream and thus maintain optimal shock position. Airflow vented to freestream through the bypass doors was also accounted for as propulsion drag. Active controls for regulating the bypass doors are beyond the scope of this work.

The inlet was instrumented with high-speed dynamic pressure sensors and slower electronic scanned pressure (ESP) transducers. The high-speed dynamic sensors had transducers mounted within the inlet that converted pressure on the sensor face to an analog voltage value that was transmitted by wire to data recorders. Within the data recorders, the voltage values were sampled and converted to pressure values

using calibration coefficients. Two sets of calibration coefficients were available for these sensors: cold (80 °F) and hot (250 °F).

Each ESP sensor was located outside of the wind tunnel test section—about 30 ft away. The input to each ESP sensor was plumbed to a pneumatic tube that attached to the measurement point of interest within the wind tunnel or inlet system. The ESP transducer signals were electronically transmitted to data recorders. For the ESP sensors, a change in pressure included a pneumatic delay as the pressure pulse moved through the tube to the transducer. Another consideration with ESP sensors was that a backpressure change resulted in pressure oscillations within the tube. Therefore, before recording ESP data, a waiting period was required to allow the oscillations to dampen out. To improve ESP accuracy, five data points were acquired at 1-s intervals and then averaged into a single measurement value. Because of the procedure to acquire ESP data, the ESP data were considered to be near steady state. At the AIP, total pressure was measured using Prati probes (Ref. 1). These probes included high-speed dynamic pressure sensors along with ESP sensors.

For the experiments being reported in this work, the MFP position and bypass door positions were remotely controlled using hydraulic machines. Feedback signals regarding MFP and bypass door positions were provided by variable resistors configured as variable voltage dividers. The voltages from the variable resistors were indicative of actuator position.

Wind Tunnel Facility

The experiments were conducted in the test section of the 10- by 10-Foot Supersonic Wind Tunnel (SWT) at the NASA Glenn Research Center (Ref. 2). This wind tunnel has the capability to continuously flow air around a circuit and through the test section at a constant Mach number, total temperature, and total pressure. These calculations and measurements were based on sensors located in the tunnel bellmouth. A typical run night with this wind tunnel would have the test section at wind-on condition continuously for 6 h. The 6-h limit was a constraint based on facility power availability and not necessarily a tunnel operating limitation. Other tunnels that may be of interest are blowdown facilities. A blowdown wind tunnel would have a defined period of wind-on condition based on the wind tunnel design—upstream air supply, downstream vacuum chamber, airflow geometry, and desired operating condition. Tests in a blowdown wind tunnel could involve multiple periods of wind-on condition with each run period typically defined in units of minutes. Operating-cost comparisons between the continuous-flow wind tunnel and blowdown wind tunnels are beyond the scope of this work. The point of emphasis here is that blowdown wind tunnel facilities with limited on-condition periods can also use the technology being presented in this work to acquire data with fewer runs.

For this work, three data recording systems were available. The first was a legacy system configured to record pressure measurements and actuator movements at near-steady-state conditions. This system was not used to capture pressure or actuator movement dynamics. Because this was a facility legacy recording instrument with considerable reliability history, this system was considered the truth for identifying near-steady-state pressure conditions and actuator positions. After all pressure oscillations dampened to near steady state, this system was able to record ESP signals, pressure signals from the high-speed dynamic pressure sensors, and actuator position signals. This system continuously measured data at 1 Hz and, upon command, five measurements were averaged and recorded: two measurements prior to the record command, one current measurement, and two measurements immediately following. In this report, this system is referred to as the “discrete system.”

The second system was designed to replace and become the new legacy system. This system was configured to record data at 200 Hz. It recorded all signals from high-speed dynamic pressure sensors as

well as all actuator positions and was designed to continuously sample data at 12.8 kHz. It used an analog anti-aliasing low-pass filter with cutoff frequency at 5 kHz. The ESP sensors, being dedicated to and recorded on the first system, were not recorded on the new system. In this report, this system is referred to as the "slow dynamic system."

The third system was a high-speed recording instrument configured to record data at 10 kHz. Signals from all high-speed dynamic pressure sensors were routed to this instrument, as well as all actuator position signals. The ESP sensors remained on the original system. The third system continuously sampled signals at 2.6 MHz and employed an analog anti-aliasing low-pass filter with cutoff frequency at 50 kHz. In this report, this system is referred to as the "fast dynamic system."

Testing procedures for this work had the slow dynamic and fast dynamic data acquisition systems activated for a period of about 30 s whenever the legacy discrete system was commanded to record. As a result, for every steady-state reading, measurements recorded on the slow and fast dynamic data recordings could be averaged and compared to the recording on the legacy discrete system.

For the Glenn SWT, four stages initiated a run session. Stage 1 had the test section at atmospheric conditions and no airflow. At stage 2, the wind tunnel test section was at a lower pressure to decrease supersonic transient loading on the test article and to decrease loading on the wind tunnel turbines during startup in the subsequent stage. In stage 3, the wind tunnel turbines were started and supersonic airflow was established in the test section. Lastly, at stage 4, the test section was on condition as defined by a desired altitude and Mach number. At the beginning of each run session, stage 1, an atmospheric pressure measurement was recorded for all pressure sensors. At stage 2, another set of pressure measurements was recorded. These two sets of recordings were acquired without airflow and were referred to as "tare readings." With no air flowing, it was expected that all the pressure sensor readings would match. In actuality, there were very small differences that could be attributed to such factors as different calibration settings or analog-to-digital conversion coefficients.

After recording the two tare measurements, the wind tunnel was started, and the experiments commenced when the desired tunnel conditions were attained. At the completion of a run session, tunnel air was exhausted to decrease pressure, and the tunnel test section was deliberately unstarted at low loading. The tunnel pressure was decreased before unstarting the tunnel test section to minimize the impact of the shock passing over the inlet system during that period. Next, the wind tunnel turbines were stopped, and another set of tare readings was taken with the wind tunnel at a quiescent low-pressure condition and then again at atmospheric conditions. The tare measurements recorded from each sensor were compared against recorded measurements from other sensors to detect sensor failures that impact posttest data analysis. A measurement value that deviated from the others during the tare stages indicated a failed sensor. Without knowledge of the time when the sensor failed, measurement data from failed sensors were withheld during data analysis.

Discrete Characteristic Curves

A notional cane curve is illustrated in Figure 2. Pressure recovery is diffuser total pressure (P_{T2}) as measured with a rake of Prati probes mounted in the flow path at the AIP, normalized with an effective freestream total pressure (P_{T0}) value. The x-axis on the cane curve is a measurement of air mass flow at the AIP (W_2) normalized by air mass captured (W_{Ref}). Values for W_2 are from airflow measurements when airflow exiting the cold pipe was choked because of the MFP position. W_{Ref} is a theoretical captured mass flow rate at the inlet entrance.

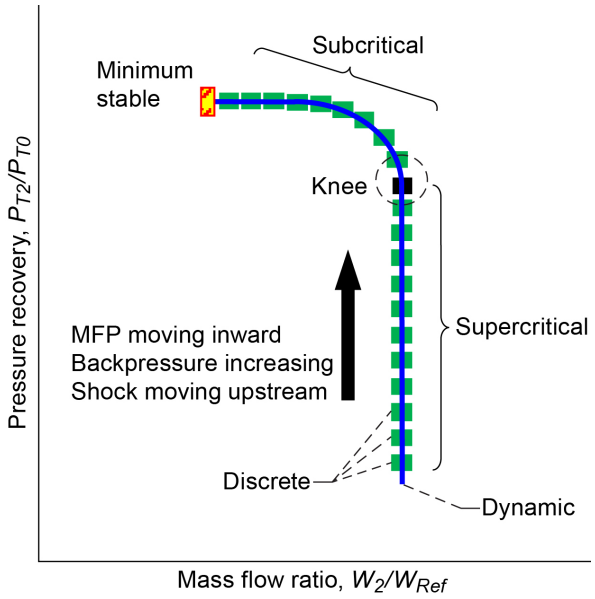

Figure 2.—Notional cane curve example.

Typically, the cane curve data collection process starts by acquiring the data points at the lower right and proceeds up and over to the upper left. The green squares in Figure 2 are an example of discrete data collected using the previous baseline process to create a cane curve. The blue continuous line is a notional representation of the same inlet at the same conditions but using the suggested dynamic data acquisition process that will be introduced in the following section.

In Figure 2, the inlet system passes through four phases: supercritical, the cane curve knee, subcritical, and minimum stable. The supercritical phase has pressure recovery increasing and mass flow ratio constant, as illustrated by the vertical segment of the notional cane curve. That relationship indicates that the normal shock wave is located downstream of the throat bleed. As the normal shock passes over the throat bleed plate, W_2 values decrease as bleed venting increases. This phase results in the data points making up the knee of the curve. A point of best performance is termed “critical” or “peak” and is suggested by the black circle and black square. Further movement of the MFP toward the cold pipe results in a maximum recovery, as represented by the top horizontal portion of the cane curve, a region termed “subcritical.” Figure 2 is notional; a real cane curve would have shown pressure recovery continuously increasing as mass flow ratio decreased instead of showing it as horizontal. The last data point, represented by the yellow and red striped square, is the minimum stable operating point. At minimum stable, further movement of the MFP to increase backpressure will cause the inlet to expel the normal shock, resulting in an unstarted condition. Due to the temporary relief of backpressure provided by the bleed plates, the inlet will restart, followed by another unstart as backpressure continues to build. The condition where the inlet repeatedly restarts and unstarts is known as the buzz condition.

Baseline Process

To acquire mixed-compression inlet performance characteristic curve data, the baseline process incrementally advanced a backpressuring actuator, such as the MFP, to positions that yielded increasing backpressure. After each incremental step, data were recorded. After progressing the backpressuring actuator beyond the minimum stable point, the inlet system would unstart. Actions were then performed to restart the inlet, and the process was completed. Postprocessing analysis reduced the recorded

measurements from specific pressure sensors and the MFP position to coordinate values for data plotting the discrete inlet performance characteristic curves.

The baseline process was initiated and completed with the bypass doors in a fixed position, preferably closed, for all data points. With the bypass doors closed, the measured W_2 was the same airflow that passed through the subsonic diffuser. If the bypass doors were partially open, the measured W_2 would be less than the airflow exiting the subsonic diffuser due to the venting loss.

Cane curve plots were generated from data recorded using the discrete recording system at each incremental step. The y-axis pressure recovery (P_{T2}/P_{T0}) used averaged values of P_{T2} from 40 ESP sensors located at the AIP. Values for P_{T0} were averaged signals from sensors in the tunnel bellmouth. Tunnel conditions were held constant while conducting experiments for a cane curve. The values for W_{Ref} were calculated based on freestream condition and inlet capture area. Values for W_2 were output from an algorithm that had input variables of MFP position (X_{MFP}), wind tunnel test section total temperature (T_T), and static pressure averaged from measurements recorded by three ESP sensors located in the cold pipe (P_{CP}). The algorithm calculations were performed by the recording instrumentation, and the data were saved in a file formatted as comma-separated values. The data files contained all information needed, without further postprocessing, for illustrating characteristic curves immediately after being recorded.

Proposed Process

The concept of waiting for ESP oscillations to dampen to near-steady-state measurements led to considerations of how to make this process faster. Could the waiting period be eliminated, and could the requirement to incrementally move the backpressuring actuator be relieved? First, the backpressuring actuator could continuously move at a constant rate to pass over the discrete positions, as illustrated in Figure 2; there was no need to wait for the X_{MFP} signal to dampen. Second, the wind tunnel conditions were held constant; therefore, it was not necessary to wait for P_{T0} measurements to reach steady state for each data point. Also, the inlet capture area was held constant while acquiring cane curve data; therefore, it was not necessary to wait for W_{Ref} values to reach steady state. However, calculations for P_{T2} used measurements from the Prati probe ESP sensors. Likewise, W_2 values were calculated using P_{CP} measurements from ESP sensors in the cold pipe.

To address these issues, a new strategy was proposed and investigated. The new strategy employed high-speed dynamic pressure sensors that would not need a delay for pressure damping because, unlike the remote ESP sensors, their pressure-sensitive surface was on location. Because the Prati probes already had high-speed pressure sensors to measure P_{T2}, those values would be available without requiring pressure oscillations to dampen to steady-state values. To calculate W_2, three additional dynamic pressure sensors were installed in the cold pipe near the P_{CP} tubes. These additional sensors would make dynamic signals available for calculating W_2 without requiring a pause for oscillations to dampen.

In the proposed new process, the bypass doors were kept in a fixed position and data were recorded by two types of dynamic data recorders while the backpressuring MFP actuator was continuously moved from supercritical to minimum stable. The dynamic data files of information were available for populating a continuous cane curve. Throughout the course of acquiring continuous cane curve data, the necessary steady-state data that did not change were recorded on the steady-state recording system. The dynamic data capturing X_{MFP}, P_{T2}, and P_{CP} measurements were recorded on the slow and fast dynamic data acquisition systems. This process collected all of the necessary data within the same timeframe needed to record a single datum point using the discrete baseline process. In this report, data acquired using the proposed process are identified as “dynamic” data, and the data acquired using the baseline process are identified as “discrete” data. The authors assert that the dynamic data approach could at

minimum be a useful tool to help inform and direct discrete data collection; regions of interest could be quickly explored to highlight where discrete data collection should be focused.

Although the proposed process acquired data more cost effectively, it did include risks and challenges. The main risk was that the numerous data points acquired might not be as accurate as the one data point acquired using the discrete data acquisition process. To validate or relieve this risk with a cost benefit assessment is beyond the scope of this work. To identify and understand other risks and implications, a study was performed with experimental wind tunnel data that compared the baseline analysis to analyses performed with data acquired using the proposed data acquisition process. For this work, "accuracy" is understood to mean how well the dynamic data matched the discrete data when comparing data points that should be equal. For example, measurements at the same freestream conditions and inlet geometry should result in identical cane curve data. Another consideration of this study was to determine if the rate of actuator movement impacts accuracy. Yet another consideration was to determine if there were dynamic effects within the data set acquired using the continuous cane curve process that were not available with data acquired using the baseline process. Also, functional details of the discrete data that have influence on its accuracy should be understood. The traditional approach uses pneumatic tubes from the flow surface to the ESP sensor module that can be several inches to tens of feet in length. This first-order effect causes a transient lag in the pressure response. Additionally, any true transient pressure fluctuation could excite further higher order oscillatory inaccuracies.

Given that both processes used the same steady-state values, such as the freestream conditions and upstream inlet geometry, the only differences in the methods for calculating characteristic curve plots were the sensors used to measure static and total pressure and the value for X_{MFP}, which continuously changed. Ideally, the pressure signals dynamically recorded as the MFP increased backpressure would be identical to the pressures measured using the discrete process when X_{MFP} were the same for both processes. The challenge for this work became an exercise to get the dynamic pressure recordings to match the steady-state pressure recordings when the time-varying X_{MFP} matched the discrete recorded value for X_{MFP}. The next section discusses a multistep approach to reduce recorded dynamic data to match the steady-state data.

Data Reduction Processes

In this section, the analysis methods employed in the study are reviewed. The methods are presented in order of increasing complexity. First, a sensor data qualification (SDQ) algorithm used to qualify measurement values is presented, followed by a description of a coefficient recalibration process that adjusted each dynamic pressure measurement to compensate for temperature variation. Next, an overview of the atmospheric tare analysis process is presented. This analysis was applied to the data after the SDQ algorithm was completed to compensate for measurement bias. Lastly, a summary of the procedure used to create cane curves from dynamic data sets is provided.

Sensor Data Qualification

This section provides a SDQ process to identify and remove from consideration any sensor data deemed corrupted or otherwise unreliable. This SDQ process compares measurements with neighboring sensors for validation, and it was applied to two sets of pressure sensors. The first pressure sensor set consisted of the 40 AIP rake measurements, and the other set contained the three cold pipe measurements. The AIP rake sensors measured total pressure, and these measurements were averaged from all signals passing the SDQ process to determine values for P_{T2} from the dynamic data. The cold pipe sensors included three static pressure sensors, and these measurements were averaged and used to calculate W_2.

For each sensor set, the SDQ algorithm employed was the same. The SDQ process determined a total error (*re*) value as the average time difference between a sensor and two adjacent sensors, as described in Equation (1). The dynamic data sets included *n* data points over a period for each sensor and let *k* identify one data point in the period. Values for *re* were determined for all sensors over the whole period. Error for the j^{th} sensor was measured by comparing values with measurements from adjacent pressure signals at the *j+1* and *j–1* sensor positions.

The final value is an average sensor error for all *n* data points acquired. All of the sensors were not expected to measure the exact same pressure values (*re* = 0). An accepted value of 40 psia was determined after inspection of experiment data. Sensors with an *re* value greater than 40 psia were disqualified.

$$re_{j,j\pm1} = \sqrt{\frac{1}{n}\sum_{k=1}^{n}\left(\frac{P_{k,j} - P_{k,j\pm1}}{P_{k,j}}\right)^2} \tag{1}$$

Coefficient Recalibration

To improve high-speed pressure measurement accuracy, a coefficient recalibration scheme was developed to account for the measured total temperature of the wind tunnel test section. In this scheme, linear interpolation was used when the test section total temperature was between the calibration temperatures of 80 and 250 °F.

While recording pressure measurements, the hot coefficients were used to translate measured voltage from the pressure transducer to psia values. The first step was to determine the pressure sensor transducer voltage that was measured from each pressure sensor as shown in Equation (2). Here, *Volts* is the calculated volts, P_{Hot} is the recorded hot pressure based on the use of the 250 °F calibration coefficients in units of psia, and $C0_{Hot}$ and $C1_{Hot}$ are the hot calibration coefficients.

$$Volts = \frac{(P_{Hot} - C0_{Hot})}{C1_{Hot}} \tag{2}$$

Next, the estimated voltage measured by the data recorder (*Volts*) was used to determine what the cold pressure measurement would be using the 80 °F calibration coefficients. As given in Equation (3), P_{Cold} is the estimated cold pressure measurement in psia, and $C0_{Cold}$ and $C1_{Cold}$ are the cold calibration coefficients.

$$P_{Cold} = C0_{Cold} + C1_{Cold} * Volts \tag{3}$$

Finally, linear interpolation was used to calculate the recalibrated pressure measurement P_{Recal} given the recorded test section total temperature T_T (°F) as displayed in Equation (4).

$$P_{Recal} = P_{Cold} + (T_T - 80)\frac{(P_{Hot} - P_{Cold})}{(250 - 80)} \tag{4}$$

This process was only applicable when the test section total temperature was within the bounds of calibration temperatures. Otherwise, the coefficient recalibration process was not expected to increase measurement accuracy.

Atmospheric Tare Analysis

The atmospheric tare data were used for two purposes: to verify pressure signal sources and to determine measurement bias compensation.

The data were used to verify the pressure signal sources for a particular wind tunnel session based on SDQ analysis of the recorded measurements on the dynamic measurement systems. The atmospheric tare data were preferred over the low-pressure tare data because sensor accuracy was considered to be highest toward the middle of the pressure sensor range. However, for the slow dynamic system in this study, it was necessary to use the low-pressure tare because the system was activated as the test section was being pumped down to the low-pressure condition. It was activated after the pause at atmospheric conditions and did not contain steady-state data.

This data set was also used to determine measurement bias compensation to offset measurement drift in the dynamic pressure sensors. With no wind in the test section, the recorded pressures were expected to be the same. Therefore, it was assumed that any deviation was due to calibration drift with the dynamic sensors. To account for this drift, a unique constant bias value for each dynamic pressure sensor was determined based on the difference between the average of the recorded dynamic pressure sensors and the nearest ESP transducer.

Cane Curve Analysis

An automated process was used to generate the cane curves and is briefly summarized here. To compare discrete and dynamic processes, the compared data sets had to have the same upstream inlet geometry and freestream conditions. This process started with a study of the SDQ analysis on the atmospheric tare data. Dynamic data recordings of tare data were not always constant values, as would be expected if the recorder was started and stopped while pressure in the tunnel test section was at a constant atmospheric pressure.

Triggering the dynamic data acquisition system was a manual process. Sometimes the recording was started too soon, before pressure stabilized, which was not a problem for the data set populated at the beginning of a run session. However, the data set at the end of a run session might include a rise in pressure while the SWT was returning to atmospheric pressure. Sometimes the recording stopped too late, in which case atmospheric tare data acquired at the beginning of a run session might include a drop in pressure at the end of the data set as the SWT startup process initiated with a pump-down process. For this part of the process, tare data sets were segmented into three periods: beginning (potentially including a pressure drop), middle (selected to be a flat period), and end (potentially including a pressure rise). Only the middle data points were applied to the SDQ process to qualify sensors and determine biases. The beginning and ends of these data sets were trimmed to eliminate pressure transients that may have been recorded before starting or stopping the dynamic data acquisition system.

The cane curve analysis continued with the following six-step process:

1. Using SDQ, identify the qualified sensors.
2. Down sample the data by applying an anti-aliasing filter. The recorded data from the fast dynamic data recorder were reduced from 0.0001 s between data points (10 kHz) to 0.01 s between data points (100 Hz)—keeping every 100th data point. Down sampling was especially necessary for the fast dynamic data to allow timely reduction and analysis of data. Likewise, data recorded on the slow dynamic recording system were down sampled. Again, an anti-aliasing filter was applied to the data. The filtered data were reduced from 0.005 s between data points (200 Hz) to 0.08 s between data points (12.5 Hz)—

keeping every 16th data point. After down sampling, measurement recalibration with respect to T_{T0} and measurement biases was applied.

3. Calculate values for W_2 for the dynamic working data points. The W_2 value was based on P_{CP}, T_T, and X_{MFP}. Units for these terms are psia, Rankine, and inches, respectively. For this work, P_{CP} and X_{MFP} were recorded on both dynamic data systems.

4. Use the dynamic working data to calculate total pressure recovery on the cane curve ordinate. At this point, the dynamic working data set also included pressure recovery, mass flow ratio, and MFP positions.

5. Compare the discrete and dynamic data at similar MFP positions. For each steady-state MFP position, the closest matching MFP position in the dynamic working data set was found. The MFP positions were similar if the difference in position between the two was less than 0.1 in.; if the difference was not less than 0.1 in., the discrete data point did not have a matching dynamic data point, and that discrete data point was removed from further consideration. Hence, the discrete working data set included all discrete data points that had MFP positions matching those in the dynamic working data set. The difference between cane curve terms for the two data sets lies in the accuracy of the pressure sensors. To quantify the difference in cane curve generation for both working data sets, an error term as defined in Equation (5) was employed. Here, m was the number of data points in the discrete working data set; $\Delta_{W,i}$ was the difference between the discrete mass flow ratio and the dynamic mass flow ratio for discrete working data point i; and $\Delta_{P,i}$ was the difference between discrete pressure recovery and the dynamic pressure recovery for discrete working data point i.

$$error = \frac{1}{n}\sum_{i=1}^{m}\sqrt{\left(\Delta_{W,i}^2 + \Delta_{P,i}^2\right)} \tag{5}$$

6. The last step was to plot the data. The data from the dynamic working group were plotted as continuous data, and the data from the discrete working group were plotted as points. To highlight where the dynamic working group data had a matching point with a discrete working group data point (i.e., similar MFP positions), an open circle was used.

This analysis entertained a third method to calculate values for the characteristic curve trace. As previously noted, short-duration (~30 s) fast and slow dynamic data were recorded along with each discrete data recording. These data were reduced to a single value using their mean values while conditions were steady state. Next, this set of data was processed in the same manner previously described to produce an additional set of discrete data points. These data points were referred to as “hybrid data” and were matched with the respective discrete data that were recorded with them. These hybrid data points were investigated because they used the same data acquisition systems and sensors as the dynamic data but were not exposed to dynamic effects from the continuous movement of the MFP, given that they were recorded during steady-state conditions. Including these measurements in the study provided insight into the influence of the data acquisition system employed and the effects of actuator dynamics.

Results

A series of cane curves was created using both discrete and dynamic working data sets from SWT experiments with similar inlet system configurations and freestream conditions. From the experiments, three variations in the rate of MFP movement for acquiring the dynamic data were available and were used. Each of these represents the basis of a test case for examination. The three rates of MFP movement were 0.16, 0.20, and 0.27 in/s.

In the investigations, along with rate of MFP movement, four other enhancement factors were scrutinized: (1) using SDQ to remove questionable sensor measurements, (2) applying sensor drift bias compensation to correct for sensor drift, (3) using coefficient recalibration adjustments based on wind tunnel test section total temperature, and (4) comparing the accuracy of the hybrid working data set with the dynamic data set. In the following sections, the impact of each of these enhancement processes is described as they are applied to the data in the test case with the 0.16-in/s MFP movement rate. This is followed by a summary of the results for the remaining two test cases.

Test Case 1

To investigate the influence of the enhancement processes on dynamic-to-discrete data agreement, focus was given to the test case with a 0.16-in/s MFP movement rate, which was the slowest of the three rates. Five types of evaluations were performed: (1) no enhancement features (i.e., rudimentary), (2) with SDQ, (3) with SDQ and sensor drift bias compensation, (4) with SDQ and coefficient recalibration, and (5) with all of the proposed enhancements: SDQ, sensor drift bias compensation, and coefficient recalibration. A summary of the results is presented in Table I, which gives the average error terms as defined by Equation (5) for the data set in question (i.e., dynamic error) and its matching hybrid data set (i.e., hybrid error).

To begin, a cane curve using the working data with no additional improvement factors was created. This is shown in Figure 3 with slow dynamic data and in Figure 4 with fast dynamic data. In each plot, there are three traces. The black trace is the dynamic data, the blue asterisks are the hybrid data points, and the red dots are the discrete data points. The black open circles on the black trace are locations where the dynamic working data set had a MFP position match with a discrete working data set point, indicating common MFP positions.

In Figure 3 and Figure 4, the slow dynamic data show general agreement with the discrete data points, whereas there is poor agreement between fast dynamic data and the discrete data. Both sets follow the trend of the discrete data points. However, the fast dynamic working set and its hybrid data set both have significant offsets to the discrete data set. These visual observations are confirmed by the error terms in Table I. The slow dynamic set had an error of 0.0183, and its hybrid error was 0.0153. The fast dynamic had a relatively large error of 0.0452, and its hybrid set had an even larger error of 0.0919. These two cane curves represent the rudimentary case with no enhancements.

TABLE I.—ERROR TERMS FOR 0.16-in/s MFP MOVEMENT RATE PROPOSED ENHANCEMENT COMPARISONS

Description	Slow dynamic		Fast dynamic	
	Dynamic error	Hybrid error	Dynamic error	Hybrid error
Rudimentary	0.0183	0.0153	0.0452	0.0919
SDQ	0.0183	0.0153	0.0182	0.0085
SDQ, bias	0.0158	0.0136	0.0182	0.0085
SDQ, recalibrate	0.0180	0.0169	0.0209	0.0113
SDQ, bias, recalibrate	0.0155	0.0123	0.0209	0.0113

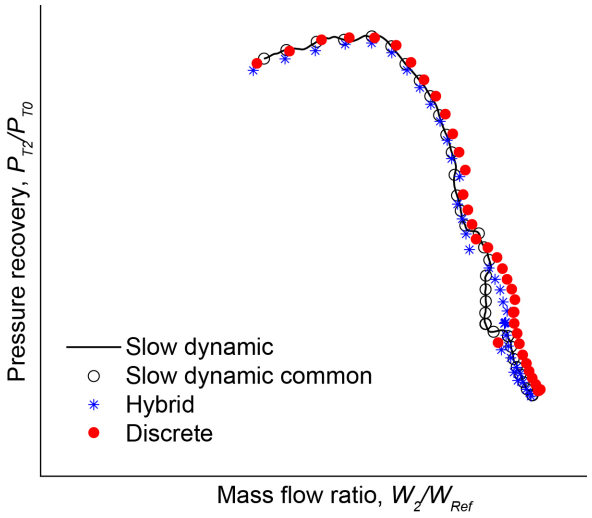

Figure 3.—Cane curve from normalized slow dynamic data with no enhancements.

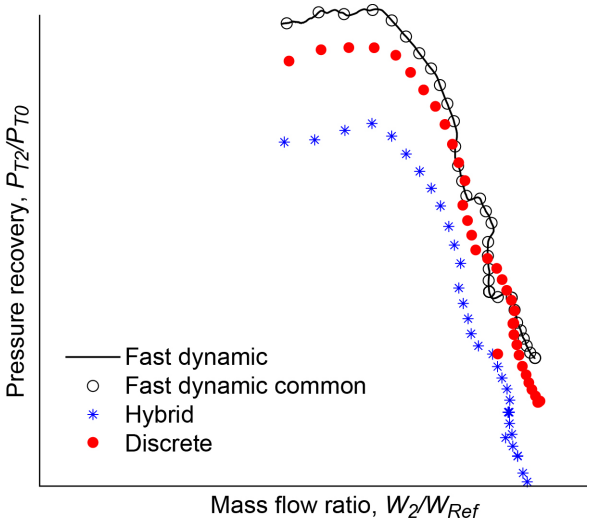

Figure 4.—Cane curve from normalized fast dynamic data with no enhancements.

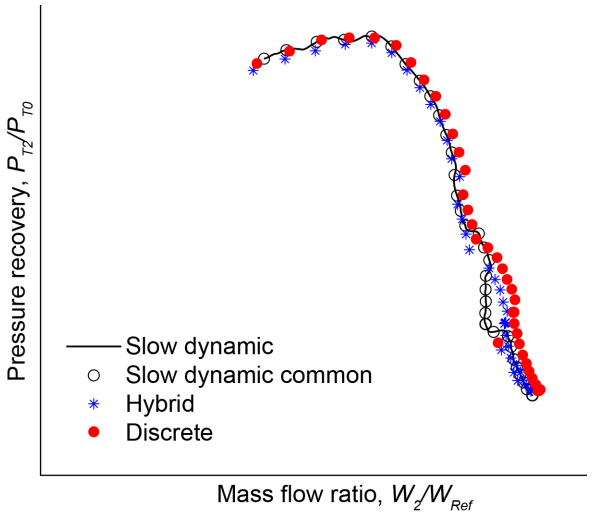

Figure 5.—Cane curve from normalized slow dynamic data with SDQ.

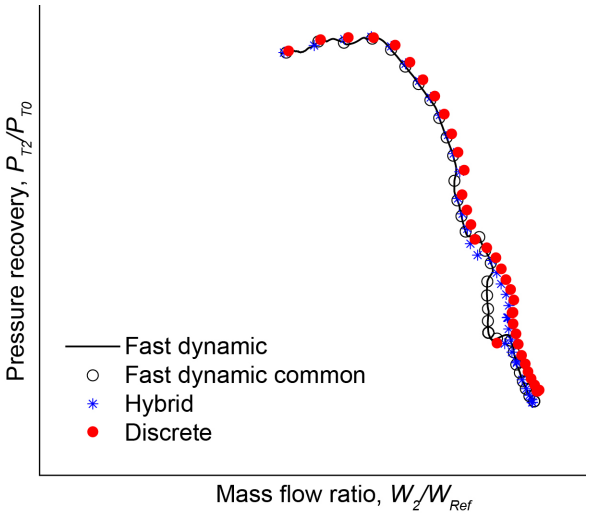

Figure 6.—Cane curve from normalized fast dynamic data with SDQ.

In Figure 5 and Figure 6, results using SDQ are illustrated. The slow dynamic data in Figure 5 appear equivalent to the slow dynamic data in Figure 3 and had the same error terms as in the rudimentary case. This was because the SDQ algorithm did not disqualify any sensors from the slow dynamic data set. Therefore, both evaluations had the same sensor set and the same data. Conversely, the fast dynamic data set in Figure 6 had a significant improvement over the fast dynamic data set in Figure 4 because one or more sensors was disqualified. Further investigation into this cause led to the illustrations in Figure 7 and Figure 8. These illustrations include traces from each dynamic sensor recorded as the MFP moved from supercritical to minimum stable. As displayed in the illustrations, the improvement was due to a single AIP rake total pressure sensor that was disqualified by the SDQ process. As shown in Figure 7, there was a noticeable total pressure measurement outlier (purple trace) that was significantly greater in magnitude than the other AIP rake sensors. This outlier sensor skewed the data along the pressure recovery axis (P_{T2}/P_{T0}) in Figure 4. In Figure 8, the outlier was removed by the SDQ algorithm, resulting in the

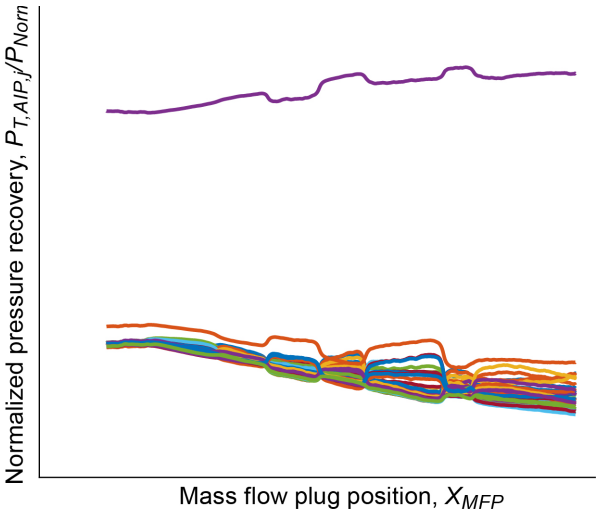

Figure 7.—Normalized AIP total pressure from fast dynamic data without SDQ.

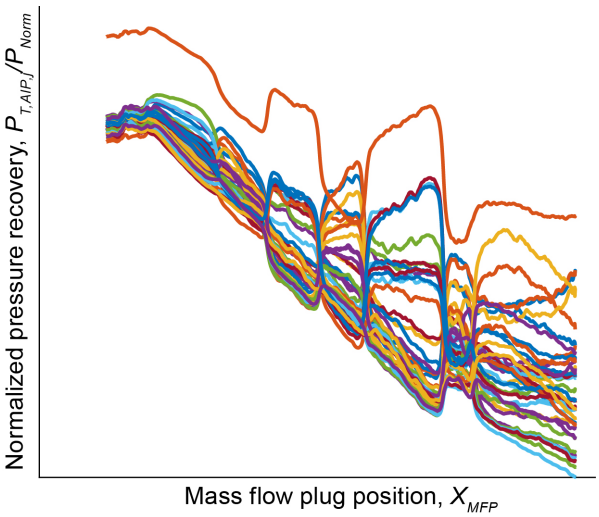

Figure 8.—Normalized AIP total pressure from fast dynamic data with SDQ.

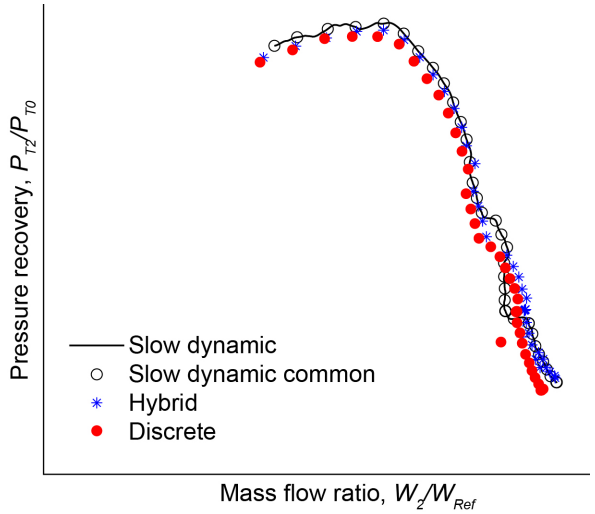

Figure 9.—Cane curve from normalized slow dynamic data with SDQ and bias compensation.

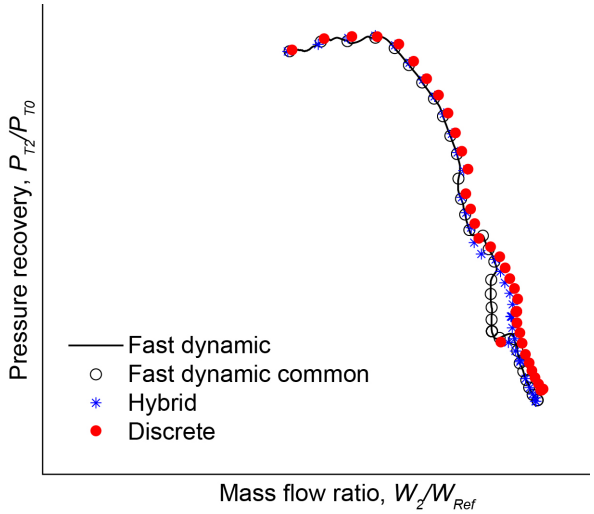

Figure 10.—Cane curve from normalized fast dynamic data with SDQ and bias compensation.

improvement seen in Figure 6. The improvement is also evidenced in Table I, where the fast dynamic data error term drops to 0.0182 and the hybrid error goes to 0.0085.

In Figure 9 and Figure 10, SDQ was performed with sensor bias compensation. As tabulated in Table I, the slow dynamic data saw a slight decrease in error, dynamic at 0.0158 and hybrid at 0.0136, and the fast dynamic data had no change in error, dynamic at 0.0182 and hybrid at 0.0085, when both are compared to their SDQ-only case.

In Figure 11 and Figure 12, SDQ and coefficient recalibration were applied, and both data sets experienced an increase in the error in comparison to the SDQ and sensor bias compensation case. The slow dynamic data sets had dynamic and hybrid errors of 0.0180 and 0.0169, and the fast dynamic data errors increased to 0.0209 and 0.0113, respectively.

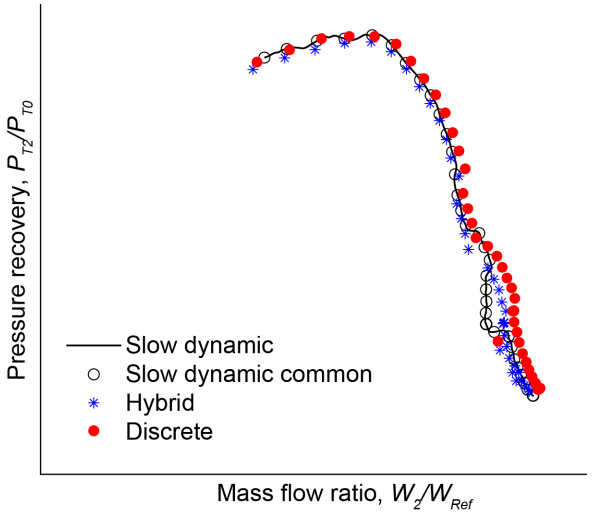

Figure 11.—Cane curve from normalized slow dynamic data with SDQ and coefficient recalibration.

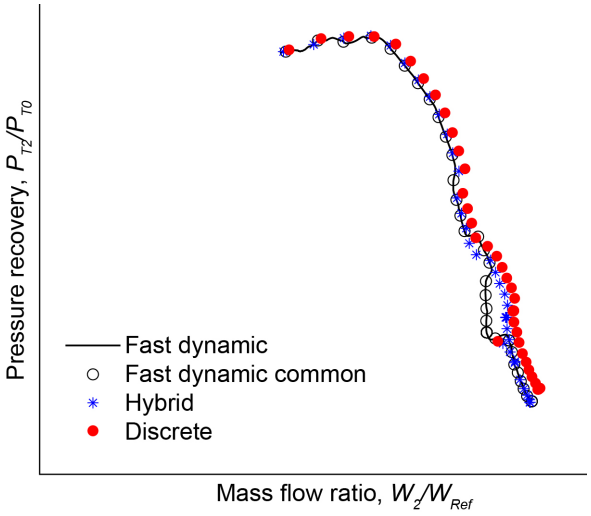

Figure 12.—Cane curve from fast dynamic data with SDQ and coefficient recalibration.

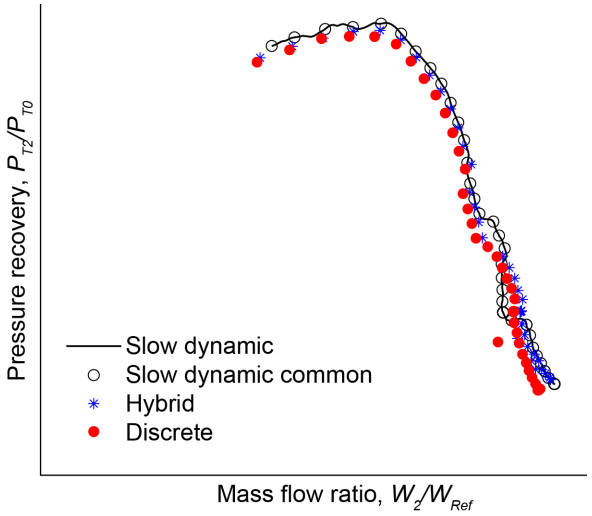

Figure 13.—Cane curve from slow dynamic data with SDQ, bias compensation, and coefficient recalibration.

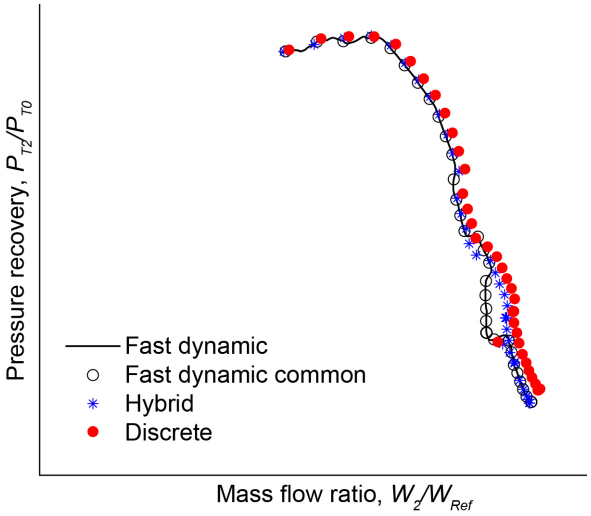

Figure 14.—Cane curve from slow dynamic data with SDQ, bias compensation, and coefficient recalibration.

Lastly, the cane curves for SDQ, sensor bias compensation, and coefficient recalibration are displayed in Figure 13 and Figure 14. The slow dynamic had the lowest overall error terms of 0.0155 for the dynamic data and 0.0123 for the hybrid data. The fast dynamic had the same error terms as the SDQ-with-recalibration case, with a dynamic error of 0.0209 and hybrid error of 0.0113.

From the curves in Figure 3 to Figure 14 and the error terms in Table I, several relevant general observations can be made that offer potential areas of further study. The slow dynamic data set along with its hybrid data had the best agreement with the discrete data when all of the enhancement processes—SDQ, sensor bias compensation, and coefficient recalibration enhancements—were employed. For both the fast dynamic and its hybrid data, the best agreement with the discrete data was in the cases of SDQ and SDQ with sensor bias compensation. Interestingly, from Table I it is apparent that the sensor drift bias compensation for the fast dynamic data did not have much effect in the cases where it was applied.

The atmospheric tare was used for the fast dynamic data, whereas the slow dynamic used the low-pressure tare. In all of the cases except for basic fast dynamic, the hybrid data for both slow and fast dynamic data sets performed the same as or better than the regular dynamic data. The best case overall was the slow dynamic with all of the enhancements.

Summary of Remaining Test Cases

Evaluations of the enhancement processes were performed on the test case with a MFP movement rate of 0.20 in/s with the error terms displayed in Table II. Data analysis showed that the slow dynamic data set had the best agreement with the discrete data when SDQ and coefficient recalibration were applied, resulting in an error of 0.0071. With an error of 0.0064, the slow dynamic hybrid had the best agreement with the discrete data when SDQ with sensor bias compensation was applied. For the fast dynamic data set, the best agreement with the discrete data was seen in the case with SDQ and sensor bias compensation, with an error of 0.0057. The fast dynamic hybrid had two cases with the best agreement with the discrete data: SDQ and SDQ with sensor bias compensation, each with an error of 0.0081. The slow dynamic data set performed better than its hybrid in three of the five cases, whereas the fast dynamic data performed better than the hybrid data in all cases.

The error terms for the test case with a MFP movement rate of 0.27 in/s are provided in Table III. Here, the slow dynamic and its hybrid had the best agreement with the discrete data with SDQ and sensor bias compensation, with errors of 0.0066 and 0.0064, respectively. The fast dynamic and its hybrid once again performed best with SDQ and SDQ with sensor bias compensation; in both cases, the dynamic error was 0.0107 and the hybrid error was 0.0084. The slow dynamic data performed better than its hybrid in all cases except for SDQ with sensor bias compensation. Conversely, the fast dynamic hybrid data performed better than the dynamic data in all cases except for the rudimentary.

Cane curve plots illustrating the best options for each test case are shown in Figure 15 to Figure 20.

TABLE II.—ERROR TERMS FOR 0.20-in/s MFP MOVEMENT RATE PROPOSED ENHANCEMENT COMPARISONS

Description	Slow dynamic		Fast dynamic	
	Dynamic error	Hybrid error	Dynamic error	Hybrid error
Rudimentary	0.0077	0.0150	0.0507	0.0913
SDQ	0.0077	0.0150	0.0058	0.0081
SDQ, bias	0.0100	0.0064	0.0057	0.0081
SDQ, recalibrate	0.0071	0.0165	0.0080	0.0108
SDQ, bias, recalibrate	0.0095	0.0069	0.0081	0.0109

TABLE III.—ERROR TERMS FOR 0.27-in/s MFP MOVEMENT RATE PROPOSED ENHANCEMENT COMPARISONS

Description	Slow dynamic		Fast dynamic	
	Dynamic error	Hybrid error	Dynamic error	Hybrid error
Rudimentary	0.0112	0.0149	0.0478	0.0917
SDQ	0.0112	0.0150	0.0107	0.0084
SDQ, bias	0.0066	0.0064	0.0107	0.0084
SDQ, recalibrate	0.0109	0.0165	0.0133	0.0112
SDQ, bias, recalibrate	0.0058	0.0070	0.0133	0.0113

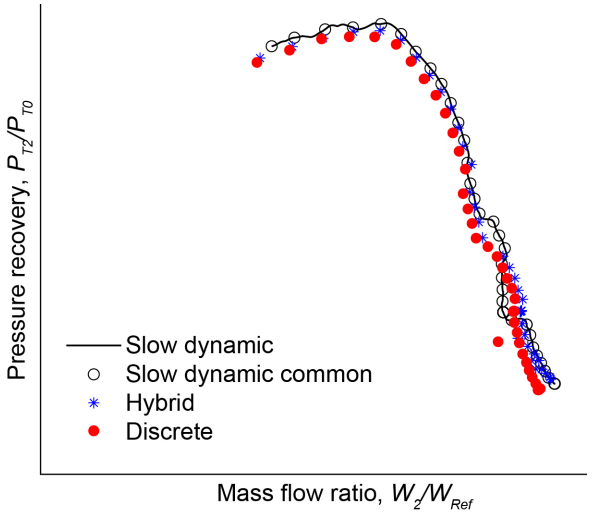

Figure 15.—Cane curve from slow dynamic data with MFP rate of 0.16 in/s with SDQ, bias compensation, and coefficient recalibration.

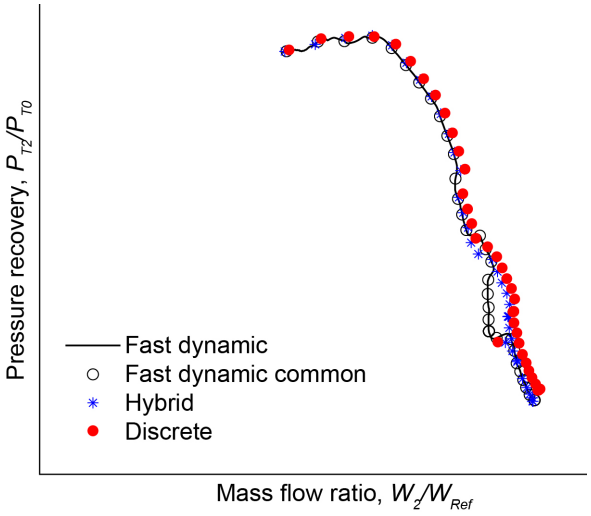

Figure 16.—Cane curve from fast dynamic data with MFP rate of 0.16 in/s with SDQ and bias compensation.

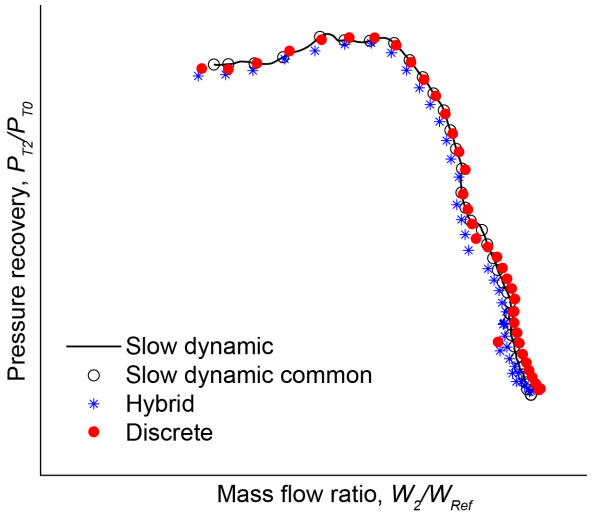

Figure 17.—Cane curve from slow dynamic data with MFP rate of 0.20 in/s with SDQ and coefficient recalibration.

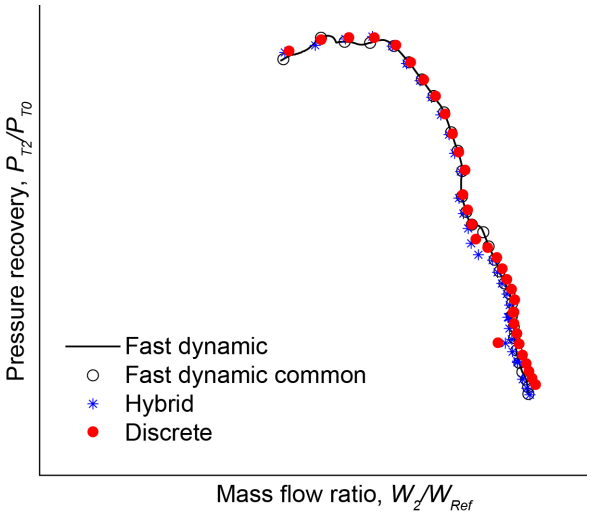

Figure 18.—Cane curve from fast dynamic data with MFP rate of 0.20 in/s with SDQ and bias compensation.

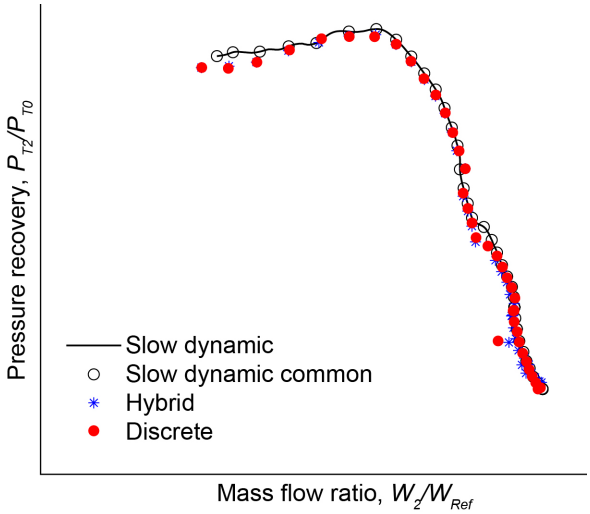

Figure 19.—Cane curve from slow dynamic data with MFP rate of 0.27 in/s SDQ, bias compensation and coefficient recalibration.

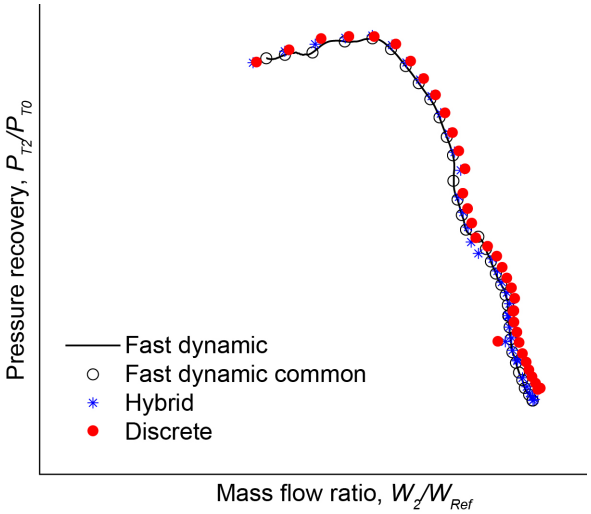

Figure 20.—Cane curve from fast dynamic data with MFP rate of 0.27 in/s with SDQ and bias compensation.

Discussion

This work examined the implications of using signals from dynamic pressure sensors instead of signals from remotely located ESP scanner modules for characterizing supersonic mixed-compression inlets. With the freestream conditions in this study unchanging as the backpressuring actuator swept throughout its range of motion, steady-state freestream data from ESP sensors were adequate and could have remained if desired. However, the ESP static pressure sensors in the cold pipe had to be augmented by three dynamic pressure sensors to obtain dynamic static pressure data. At the AIP, data from 40 dynamic total pressure transducers were used instead of data from 40 steady-state ESP sensors. The cost to procure and install these individual dynamic pressure transducers was not addressed in this study, nor was their robustness.

In the cane curve plots, Figure 3 to Figure 6 and Figure 9 to Figure 20, it is evident that the cane curves do not have the straight vertical appearance expected at supercritical operation as illustrated in Figure 2. Instead, the curves have a negative slope, or lean, to them. The lean implies that there was decreasing mass flow through the cold pipe as pressure recovery increased while the inlet was operating in the supercritical region. In the SWT experiments performed for this study, the bypass doors were not closed and sealed, thus providing a path for airflow to be vented to freestream rather than passing through the cold pipe as the MFP moved upstream and backpressure increased. Also, mass flow measurement was considered less accurate because of high levels of spatial and temporal distortion in the supercritical region. Because supercritical is not a normal operating condition, this leaning did not warrant further consideration.

In determining the sensor bias compensation values for the slow dynamic system, the low-pressure tare was used instead of the preferred atmospheric tare. During the session of wind tunnel experiments when all of the data presented in this report were recorded, the slow dynamic system was activated to record data as the test section was in the process of being pumped down to a lower pressure. Therefore, the data were not steady state, and the atmospheric tare could not be used. Instead, the bias values were determined from the low-pressure tare that was recorded a few moments later at steady state. The impact this had on bias compensation effectiveness is uncertain and is an area of further study. For the fast dynamic data, the atmospheric tare was successfully recorded at steady state and was used for bias compensation.

In many of the cane curve plots, particularly in Figure 15 and Figure 16, the dynamic data deviate from the steady-state data in the supercritical region. The dynamic data trace has a deviation to the left, indicating a sudden decrease in mass flow ratio that does not correspond to most of the discrete steady-state data points. Furthermore, there is a single rogue discrete steady-state data point that is located to the left of the main curve, also indicating a decrease in mass flow ratio, but the remaining discrete steady-state data points continue in an upward direction. The deviation appears in both the slow and fast dynamic data cane curves. This phenomenon is not apparent in the faster rates of MFP movement (i.e., 0.20 or 0.27 in/s) for either of the dynamic data cane curves. The slow and fast dynamic data illustrated in Figure 15 and Figure 16 were acquired at the exact same time. Therefore, an event may have occurred that was not repeated when the data were acquired for the other test cases. Again, being in the supercritical region, this anomaly is outside normal operating conditions of interest and did not warrant further consideration. Another anomaly is seen in Figure 8, which plots the total pressure at the AIP rake versus MFP position. Given the considerable spread of the pressure traces and the patterns of their trajectory corresponding to MFP movement in the plot, distortion is suspected. To fully understand the source of this anomaly, further study is required.

The rate of actuator movement appears to have an indeterminate influence upon measurement system agreement in the range explored in the three test cases. The error term, as expressed in Equation (5), is given in Table I to Table III for each cane curve comparison as a tool to define accuracy. Looking at the evaluations that used all of the process enhancements, there is a trend where the slow dynamic data are improving with faster MFP movement. The slow dynamic data had error values of 0.0155, 0.0095, and 0.0058 for 0.16 in/s, 0.20 in/s, and 0.27 in/s, respectively. For the fast dynamic data, the results were mixed, with error values of 0.0209, 0.0081, and 0.0133, respectively. A partial explanation for this trend may be the anomaly deviation seen in the 0.16-in/s dynamic data, as previously described. For this case, the anomaly deviation increased the error values because the discrete data were not affected by the event. Further studies may determine if there is a relationship between rate of actuator movement and measurement agreement accuracy. It may be found that slower MFP rates improve on the calculation errors, or that faster MFP rates accomplish the data collection more quickly with the same level of accuracy. Further studies may also discover how fast the MFP can move and still acquire good data and may ascertain how fast is too fast.

Analysis of the data in this study indicated good agreement between cane curves using dynamic data and cane curves from discrete data, provided the dynamic data were properly processed. The traces in the plots tend to follow common general patterns, with the noted exception of the anomaly in the slowest rate of MFP movement. Furthermore, each of the dynamic data sets was acquired in about 30 s, whereas acquisition of the discrete data took approximately 10 min using an automated data collection process as opposed to a slower manual one. If accuracy is of the essence and the quality of the dynamic data analysis is insufficient, at minimum this work suggests there is potential for the dynamic data collection process to serve as a screening tool to focus and acquire a few high-quality data points using the discrete data collection process.

Potential Future Activities

From this study, a number of items were noted that warrant further investigation. A partial listing of candidate follow-on study items is presented here.

- Directly compare the individual ESP measurements to the dynamic pressure measurements. In particular, examine Prati probe measurements because the ESP and dynamic pressure sensors are co-located.

- Repeat the wind tunnel experiments with the bypass doors closed. In the data used in this study, the bypass doors were not closed, allowing for mass flow to be vented to the freestream as backpressure increased. Therefore, the cane curves did not have a vertical trace in the supercritical region but rather displayed a negative slope lean.
- Explore the tare values used for sensor drift compensation. In this study, it was assumed that bias values derived from the atmospheric tare recorded at the beginning of a wind tunnel session were preferred. It is possible that the low-pressure tare or even either the atmospheric or low-pressure tare recorded at the end of the wind tunnel session would be more appropriate and would lead to more accurate results.
- Further investigate the effect of the distortion anomaly on the 16-in/s data set. The distortion anomaly in the 16 in/s test case caused an increase in error that made comparisons between the various rates of MFP movement indeterminate. The anomaly caused more error in the 0.16 in/s case than in the 0.20 or 0.27 in/s cases, making a good comparison difficult. Further investigations into this data set may reveal a cause.
- Repeat the wind tunnel experiments with more variation in the rate of MFP movement. The results implied improved agreement between the discrete and dynamic data sets as the rate of MFP movement increased, which is counter to the expected better agreement with slower MFP movement. By expanding the range of rate of MFP movement, this relationship can be better understood.
- Investigate why the hybrid data seemed to have better agreement with the discrete data than the dynamic data in some cases, but not as well in others. The data could be examined in detail to see how the use of dynamic data acquisition systems and actuator dynamics affect the agreement between the dynamic data and the hybrid data.
- Perform measurement uncertainty analysis to determine range of error. Each sensor and data acquisition system has sources of error due to a number of influences. Uncertainty analysis can help in understanding how close an agreement is possible and good enough for reporting.

Concluding Remarks

A study was performed to determine whether dynamic data could be used to improve data acquisition efficiencies for supersonic wind tunnel analysis of mixed-compression inlet systems. Experimental data from the 10- by 10-Foot Supersonic Wind Tunnel at the NASA Glenn Research Center were used to construct inlet characteristic curves for a mixed-compression supersonic inlet. Slow and fast dynamic data acquisition systems were used to acquire data that were then reduced to cane curves and compared to data sets created from a discrete data acquisition system. Additionally, enhancement processes were considered as a means to improve dynamic measurement quality.

The study indicated that the dynamic cane curves showed good agreement with discrete cane curves, provided they were properly processed. Requirements of the intended application dictate whether the agreement is sufficient. Furthermore, the dynamic data acquisition procedure was a less costly approach because all of its data were acquired within the same period as the data acquired for one data point using the discrete data acquisition procedure. At minimum, the process to acquire dynamic data for reduction to characteristic curves could be used to explore regions of interest that can then be further examined by discrete data collection.

References

1. Arend, David J.; and Saunders, John D.: An Experimental Evaluation of the Performance of Two Combination Pitot Pressure Probes. NASA/TM—2009-215632 (AIAA 2009–1073), 2009. https://ntrs.nasa.gov
2. Soeder, Ronald H., et al.: User Manual for NASA Glenn 10- by 10-Foot Supersonic Wind Tunnel. NASA/TM—2004-212697, 2004. https://ntrs.nasa.gov